Inorganic Chemistry

pubs.acs.org/IC Article

Selective Chromium(VI) Trapping by an Acetate-Releasing Coordination Polymer

Cambell S. Conour, Daniel G. Droege, Beatriz Ehlke, Timothy C. Johnstone, and Scott R. J. Oliver*



Cite This: Inorg. Chem. 2022, 61, 20824–20833



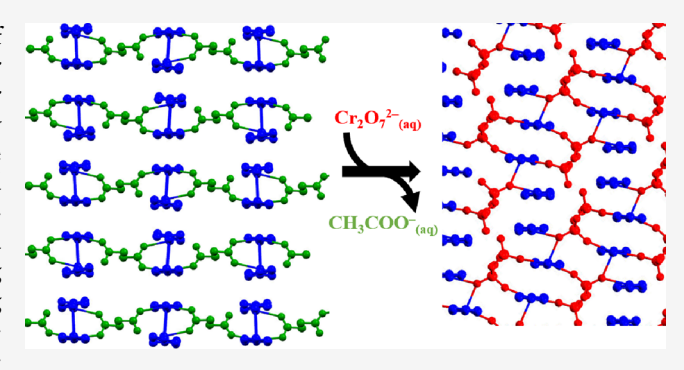
ACCESS

III Metrics & More

Article Recommendations

SI Supporting Information

ABSTRACT: We report the high-capacity and selective uptake of Cr(VI) from water using the coordination polymer silver bipyridine acetate (SBA, $[Ag(4,4'\text{-bipy})][CH_3CO_2]\cdot 3H_2O)$. Cr capture involves the release of acetate, and we have structurally characterized two of the product phases that form: silver bipyridine chromate (SBC, SLUG-56, $[Ag(4,4'\text{-bipy})][CrO_4]_{0.5}\cdot 3.5H_2O)$ and silver bipyridine dichromate (SBDC, SLUG-57, $[Ag(4,4'\text{-bipy})][Cr_2O_7]_{0.5}\cdot H_2O)$. SBA maintains a high Cr uptake capacity over a wide range of pH values (2–10), reaching a maximum of 143 mg Cr/g at pH 4. This Cr uptake capacity is one of the highest among coordination polymers. SBA offers the additional benefits of a one-step, room temperature, aqueous synthesis and its release of a non-



toxic anion following Cr(VI) capture, acetate. Furthermore, SBA capture of Cr(VI) remains >97% in the presence of a 50-fold molar excess of sulfate, nitrate, or carbonate. We also investigated the Cr(VI) sequestration abilities of silver 1,2-bis(4-pyridyl)ethane nitrate (SEN, $[Ag(4,4'-bpe)][NO_3]$) and structurally characterized the silver 1,2-bis(4-pyridyl)ethane chromate (SEC, SLUG-58, $[Ag(4,4'-bpe)][CrO_4]_{0.5}$) product. SEN was, however, a less effective Cr(VI) sequestering material than SBA.

1. INTRODUCTION

As the world becomes more industrialized, increasing levels of pollutants are released into waterways and groundwater. One of the more concerning inorganic pollutants is Cr(VI). In China, Cr-polluted land is reported to exceed 1.1% of the total land area. In the United States, Cr is cited as the second most abundant inorganic contaminant in waterways and is found at varying levels in the drinking water of every state.² Furthermore, Cr ranks among the top 20 toxic substances found within Superfund-controlled sites.³ Although Cr can be released from natural sources, modern Cr pollution stems largely from chemical and dye manufacturing, industrial energy production, leather industries, and mining.4-7 The global release of Cr into water is reported to be as high as 157,000 t per year, making it the most common pollutant in groundwater among toxic trace elements. 4,8 Cr can exist in several oxidation states, but the two states most pertinent in natural bodies of water and wastewater are Cr(III) and Cr(VI).^{4,6-9}

While Cr(III) occurs naturally and functions as an essential trace micronutrient, Cr(VI) has garnered particular concern as an anthropogenic pollutant due to its greater solubility in water and toxic effects on plants, animals, and microorganisms.^{3,4,9-12} In fact, Cr(VI) is reportedly 300–500 times more toxic than Cr(III); the human health impacts vary from irritation to cancer development, depending on exposure level.^{4,9-12} Additionally, Cr hampers the vitrification step in the processing of low-activity radioactive waste because it forms spinels in the glass, leading to degradation.¹³ The

removal of Cr(VI) is a challenge not only because of its high solubility but also because contaminated water can contain a wide array of concentrated inorganic species (such as nitrate and sulfate) and can assume a range of pH values. ^{7,14} Thus, there is great need for methods to selectively and rapidly remove Cr(VI).

Current remediation strategies include chemical reduction, electrocoagulation, bioremediation, selective crystallization, and ion exchange processes. Although chemical reduction with zero-valent iron is highly efficient, this approach lacks stability and the iron nanoparticles employed can lead to ecotoxicological effects. Electrocoagulation, while also efficient, requires skilled expertise for implementation and costly electrodes. Bioremediation is more ecologically friendly but can be inhibited at high pollutant concentrations. Traditional methods of ion exchange involving ion-exchange membranes and resins offer poor stability and selectivity. Additionally, the materials can rapidly become exhausted and be prohibitively expensive to regenerate, leading to waste generation. Even modern classes of sorbents such as

Received: August 31, 2022 Published: December 9, 2022





modified layered double hydroxides (LDHs) and zeolites can display poor adsorption efficiency and selectivity. ¹⁰

Ion exchange via coordination polymers (CPs) can offer high selectivity and straightforward material synthesis. 3,4,17-19 CPs are composed of metals linked through dative bonds with organic compounds ("linkers"), creating 1D, 2D, or 3D (metal-organic framework, MOF) extended structures. 6,20 The framework is often porous, but the pores may be occupied with charge balancing ions or solvent molecules. Interpenetration can also reduce the effective porosity of a reticular material. The physicochemical properties and reactivity of CPs have led to their potential application in a variety of fields, including gas adsorption, catalysis, and drug delivery.⁶ The ease with which CPs can be drastically altered through the selection of different metals, organic linkers, and synthetic strategies makes them attractive candidates for further development in these areas. When the CP bears an overall cationic charge, the framework requires charge balancing anions. If weakly interacting anions are appropriately chosen, then the material may be able to engage in anion exchange. Cationic CPs have already been shown to undergo selective exchange for a variety of anions. 6,17,19,21-29

Cationic silver 4,4'-bipyridine (4,4'-bipy) CPs (SBX, X = initial charge balancing anion) have previously demonstrated rapid and high-capacity anion exchange for perchlorate, permanganate, perrhenate, nitrate, acetate, tetrafluoroborate, and pertechnetate. 18,22,30,31 We have previously observed that SLUG-35 ($[Zn_{1-x}Co_x(H_2O)_4(4,4'-bipy)_2](O_3S-C_2H_4-SO_3)$. 4H₂O), a Co-Zn solid solution, was able to exchange its ethanedisulfonate anion for chromate with a capacity of 430 mmol/mol.⁶ More recently, we reported that SBA (A = acetate) exchanged acetate for perchlorate with a capacity of 99.9% mol/mol after 48 h. 18 SBA has the additional benefit of exchanging acetate (which is non-toxic) for a variety of toxic anions, as well as an extremely straightforward, scalable, and green aqueous synthesis. Here, we report the exchange properties of SBA for Cr(VI) oxo-anions as well as the discovery of several post-exchange crystal structures. The uptake performance is compared to recently published CPs and MOFs that sequester Cr. Additionally, in order to better understand the structural factors of SBA that allow for excellent Cr(VI) exchange, a related Ag(I) CP, SEN $([Ag(bpe)]NO_3, bpe = 1,2-bis(4-pyridyl)ethane), was also$ investigated and the structure of one of its post-exchange products was determined.

2. METHODS

- **2.1. Reagents.** Silver nitrate (AgNO₃, Fisher, 99.95%), silver acetate (AgCH₃CO₂, Fisher, 99%), 4,4'-bipy ($C_{10}H_8N_2$, Combi-Blocks, 97%), and bpe ($C_{12}H_{12}N_2$, Sigma-Aldrich, 99%) were used as purchased for synthesis. Potassium chromate (K_2CrO_4 , Fisher, 99.9%), sulfuric acid (H_2SO_4 , Fisher, 95 to 98% w/w), sodium hydroxide (NaOH, Fisher, 98.5%), sodium sulfate anhydrous (Na₂SO₄, Fisher, 99.5%), sodium nitrate (NaNO₃, Fisher, 99.0%), and sodium bicarbonate (NaHCO₃, Fisher, 99.7%) were used as purchased for anion exchange studies.
- **2.2. General.** All syntheses were carried out under ambient conditions unless otherwise stated. All aqueous solutions were prepared in ultrapure deionized water (>17.83 $\mathrm{M}\Omega\cdot\mathrm{cm}$). Powder X-ray diffraction (PXRD) was performed with a Rigaku Americas MiniFlex Plus diffractometer, scanning from 2 to 35° (2 θ) at a rate of 1°·min⁻¹ with a 0.02° step size using Cu K α radiation (λ = 1.5418 Å). Fourier transform infrared spectroscopy (FT-IR spectroscopy) was performed using a PerkinElmer Spectrum One spectrophotometer

with KBr pellets. UV—vis analysis was measured with a Hewlett-Packard model 8452A UV—vis spectrophotometer. Inductively coupled plasma—optical emission spectrometry (ICP-OES) was performed using a PerkinElmer Optima 4300DV, run in radial mode and using yttrium as an internal standard. Thermogravimetric analysis (TGA) was obtained via a TA Instruments Q500 TGA under a $\rm N_2$ purge and with a gradient of 5 $\rm ^{\circ}C \cdot min^{-1}$ over a range of 22–500 $\rm ^{\circ}C$

- **2.3.** Synthesis of [Ag(4,4'-Bipy)][CH₃CO₂]·3H₂O (SBA). A mixture of 4,4'-bipy (0.330 g, 2.00 mmol) and Ag(CH₃CO₂) (0.310 g, 2.00 mmol) in 40 mL of water was stirred at room temperature for approximately 1 h. The resulting colorless microcrystalline solid was collected via vacuum filtration and rinsed with water and acetone, following previously described procedures (yield: 0.6198 g, 82% based on AgCH₃CO₂). The identity of the product was confirmed by comparison of the PXRD from the product to previously reported PXRD data (Figure S1). The identity of the product to previously reported PXRD data (Figure S1).
- **2.4. Synthesis of [Ag(4,4'-Bipy)][NO₃] (SBN).** A mixture of 4,4'-bipy (0.1560 g, 1.000 mmol) and Ag(NO₃) (0.1699 g, 1.000 mmol) in 20 mL of water was stirred at room temperature for approximately 90 min. The resulting colorless microcrystalline solid was collected via vacuum filtration and rinsed with a minimal amount of water before air-drying (yield: 0.2645 g, 81% based on AgNO₃). The identity of the product was confirmed by comparison of the PXRD from the product to predicted PXRD generated from a previously reported structure (Figure S1).³²
- **2.5. Synthesis of [Ag(4,4'-Bpe)][NO₃] (SEN).** A mixture of bpe (0.1842 g, 1.000 mmol) and Ag(NO₃) (0.1699 g, 1.000 mmol) in 20 mL of water was stirred at room temperature for approximately 90 min. The resulting colorless microcrystalline solid was collected via vacuum filtration and rinsed with a minimal amount of water before air-drying (yield: 0.3344 g, 94% based on AgNO₃). The identity of the product was confirmed by comparison of the PXRD from the product to predicted PXRD generated from a previously reported structure (Figure S1).³³ Single crystals of SEN for SEM imagery were synthesized following previously reported methods.³³
- **2.6. Chromate Uptake.** SBA (0.0471 g, 0.125 mmol), SBN (0.0404 g, 0.125 mmol), or SEN (0.0443 g, 0.125 mmol) was added to 50 mL of a 2.5 mM chromate solution. The mixture was stirred at room temperature for 1 h. UV—vis spectra of the supernatants were acquired to assess the ability of each of the three materials to deplete chromate ($\lambda_{\rm max} = 372$ nm) from the solution.
- **2.7. Effect of pH on Exchange.** SBA (0.0471 g, 0.125 mmol) was added to a $K_2\text{CrO}_4$ solution (2.5 mM, 50 mL) of varying pH values (2, 4, 5, 7, or 10) prepared through the addition of concentrated $H_2\text{SO}_4$ or NaOH with mild stirring under ambient conditions. Aliquots of approximately 1 mL were taken at 0 h (i.e., before the addition of SBA) and 24 h and filtered through a 0.22 μ m nylon filter. The filtrate was then analyzed by ICP-OES, and a standard curve was used to quantify the concentration of Cr. Exchange experiments were performed in triplicate, and the average value for each was reported.
- **2.8. Exchange Kinetics.** In a typical exchange experiment, the desired CP (SBA, SBN, or SEN, 0.125 mmol) was added as synthesized to a chromate solution (2.5 mM, 50 mL, pH was modified via the addition of concentrated $\rm H_2SO_4$, as necessary) with mild stirring under ambient conditions. Aliquots of approximately 0.5 mL were then taken at pre-determined times to monitor the exchange. At the time of sampling, aliquots were filtered through a 0.22 μ m nylon filter. The filtrate was then analyzed by UV—vis or ICP-OES, in both cases using a standard curve to quantify the concentration of Cr. Exchange experiments were performed in triplicate, and the average value for each was reported.

Exchange reactions were analyzed via a pseudo-second-order kinetics model expressed by eq (1): $Q_t = \frac{k_2 Q_e^2 t}{1 + k_2 Q_e t}$ in which Q_t is the Cr uptake in milligrams per gram at time t, Q_e is the Cr uptake at equilibrium, and k_2 is the pseudo-second-order rate constant. Q_t was calculated via eq (2): $Q_t = \frac{(C_0 - C_t)V}{m}$ in which C_0 and C_t are the

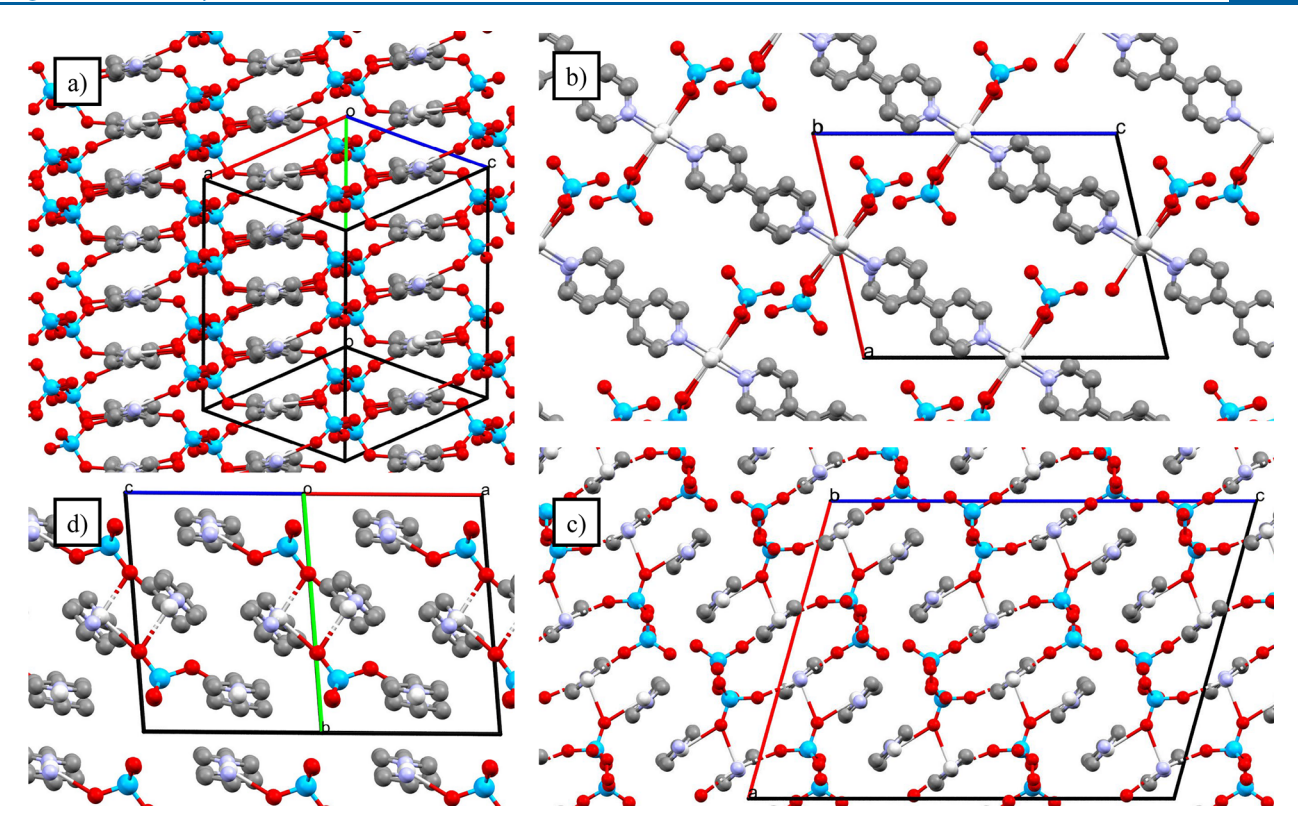


Figure 1. Structure views of (a) SBC viewed along [141], (b) SBC viewed along the *b*-axis, (c) SBDC viewed along the *b*-axis, and (d) SEC viewed down [101] (with disordered C atoms removed for clarity). All interlamellar water molecules and H atoms are omitted for clarity. Ag: silver; C: gray; O: red; N: blue; Cr: cyan. Structure views of the previously published structures of SBA, SBN, and SEN are shown in Figure S4.

concentrations initially and at time t, respectively, V is the volume of the solution, and m is the mass of the initial CP. The initial sorption rate, h, was calculated via eq (3): $h = k_2 Q_e$.

The exchange reactions were also analyzed via a pseudo-first-order kinetics model expressed by eq (4): $\ln\left(\frac{Q_e}{Q_e-Q_t}\right)=k_1t$, in which Q_e is calculated via eq. 1 and k_1 is the pseudo-first-order rate constant.

2.9. Exchange Capacity. SBA (0.0235 g, 0.0625 mmol) was added to a K_2 CrO₄ solution (50 mL) of varying initial concentrations (0.5, 1.25, 2.5, 5.0, and 10.0 mM) with mild stirring under ambient conditions. Aliquots of approximately 1 mL were taken at 0 and 24 h and filtered through a 0.22 μ m nylon filter. The filtrate was then analyzed by ICP-OES, and a standard curve was used to quantify the concentration of Cr. The exchange experiments were performed in triplicate, and the average value for each was reported.

Exchange data were then fitted to a Langmuir model expressed by eq (5): $\frac{C_{\rm e}}{q_{\rm e}} = \frac{1}{q_{\rm m}b} + \frac{C_{\rm e}}{q_{\rm m}}$ in which $C_{\rm e}$ is the concentration of aqueous-phase adsorbate ions at equilibrium (mg/L), $q_{\rm m}$ is the maximum adsorption capacity (mg/g), $q_{\rm e}$ is the uptake of adsorbate at

Exchange data were also fitted to a Freundlich model expressed by eq (6): $\ln(q_e) = \ln(K_f) + \left(\frac{1}{n}\right) \ln(C_e)$ in which K_f is the Freundlich constant and $\frac{1}{n}$ is the heterogeneity factor.

equilibrium (mg/L), and b is the Langmuir model constant (L/mg).

2.10. Growth of Single Crystals of [Ag(4,4'-Bipy)][CrO₄]_{0.5'} 3.5H₂O (SBC, SLUG-56). SBN (0.0404 g, 0.125 mmol) was suspended in 50 mL of a 2.5 mM chromate solution and stirred at room temperature for 24 h. The suspended solid was collected by filtration, rinsed with a minimal amount of water, and dried. Approximately 5 mg of this post-exchange material was then added to 5 mL of water. Concentrated aqueous ammonia was then added in a dropwise manner until the solid was completely dissolved. The solution was then allowed to evaporate over the course of several days to afford diffraction-quality crystals.

2.11. Growth of Single Crystals of [Ag(4,4'-Bipy)][Cr₂O₇l_{0.5'} H_2O (SBDC, SLUG-57). SBN (0.0404 g, 0.125 mmol) was suspended in 50 mL of a 2.5 mM chromate solution, the pH of which was adjusted to 4 via addition of H_2SO_4 . The suspension was stirred at room temperature for 24 h. The suspended solid was collected by filtration, rinsed with a minimal amount of water, and dried. Approximately 5 mg of this post-exchange material was then added to 1 mL of a concentrated aqueous dichromate solution. Acetonitrile was then added in a dropwise manner until the solid was completely dissolved. The solution was then allowed to evaporate over the course of several days to afford diffraction-quality crystals.

2.12. Growth of Single Crystals of [Åg(4,4'-Bpe)][CrO₄] $_{0.5}$ (SEC, SLUG-58). SEN (0.0443 g, 0.125 mmol) was suspended in 50 mL of a 2.5 mM chromate solution and stirred at room temperature for 24 h. The suspended solid was collected by filtration, rinsed with a minimal amount of water, and dried. Approximately 5 mg of this post-exchange material was then added to 5 mL of water. Concentrated aqueous ammonia was then added in a dropwise manner until the solid was completely dissolved. The solution was then allowed to evaporate over the course of several days to afford diffraction-quality crystals.

2.13. Selectivity. Selectivity studies were performed by mixing SBA (0.0471 g, 0.125 mmol) in a Cr(VI) solution (50 mL, 2.5 mM) at pH 4 (pH modified via the addition of concentrated $\rm H_2SO_4$) with a molar ratio of 1:50 (Cr: competing anion). Aliquots of approximately 1 mL were taken before the addition of SBA and at 24 h. The competing ions were sulfate ($\rm SO_4^{2-}$), carbonate ($\rm CO_3^{2-}$), or nitrate ($\rm NO_3^{-}$). At the time of sampling, aliquots were filtered through a 0.22 μ m nylon filter. The filtrate was then analyzed via ICP-OES, and a standard curve was used to quantify the concentration of Cr.

2.14. Solubility. Solubility studies were performed by adding approximately 40 mg of the desired CP in 25 mL of water, producing a saturated solution. The solutions were allowed to reach equilibrium for 10 d before an aliquot was taken, filtered through a 0.22 μ m nylon filter, and analyzed by ICP-OES. A standard curve was used to

quantify the concentration of Ag. The analysis of each material was performed in triplicate, and the average value was reported.

2.15. X-ray Crystallography. Crystals of SLUG-56, SLUG-57, and SLUG-58 were grown as described above. Single crystals suitable for X-ray diffraction were selected under a microscope, loaded onto a nylon fiber loop using Paratone-N, and mounted onto a Rigaku XtaLAB Synergy-S single crystal diffractometer. Each crystal was cooled to 100 K under a stream of nitrogen. Diffraction of Cu K α radiation from a PhotonJet-S microfocus source was detected using a HyPix-6000HE hybrid photon counting detector. Screening, indexing, data collection, and data processing were performed with CrysAlisPro.³⁴ The structures were solved using SHELXT and refined using SHELXL as implemented in Olex2 following established strategies.^{35–38} Unless otherwise specified in the CIF, all non-H atoms were refined anisotropically and H atoms were placed at calculated positions and refined with a riding model and coupled isotropic displacement parameters. Refinement parameters are given in Table S1.

3. RESULTS AND DISCUSSION

3.1. Chromate Exchange and Characterization of **Exchange Products.** The acetate- and nitrate-containing CPs SBA, SBN, and SEN all demonstrated an ability to sequester Cr(VI) from an aqueous solution in which they were suspended. When any of the three CPs was suspended in a 2.5 mM chromate solution, the absorption arising from the Cr(VI) oxyanions ($\lambda_{max} = 372$ nm) was gradually depleted over the course of 1 h (Figure S2). In an effort to further understand the products that formed following this uptake of Cr(VI), diffraction-quality single crystals of the materials formed by the exchange were grown and their structures were determined via X-ray diffraction, as well as imaged via SEM (Figure S3). The product of the Cr(VI) exchange by SBN under acidic conditions (pH 4) was also collected, used to form diffraction-quality single crystals, and its structure was determined via X-ray diffraction and imaged via SEM (Figure S3).

The uptake of Cr(VI) oxyanions is theorized to occur through solvent-mediated crystal-to-crystal ion exchange in which the starting material dissolves into the solvent and then recrystallizes with the exchanged ion, as is typically observed in 1D CPs and was previously demonstrated for SBN.³⁹ This theory of dissolution and precipitation is supported by the differing morphologies between the pre- and post-exchange materials observed in SEM imagery. SBA crystals have previously been shown to have a thin, rectangular plate morphology, and SEN crystals appear as blocky rods (Figure S3a). 18 This is in contrast to SBC, which grows as packed, thin needles (Figure S3b), SEC, which grows as thicker, splintered rods (Figure S3c), and SBDC, which displays two predominant morphologies: non-rectangular thin plates as well as blockier rods (Figure S3d). Given this proposed exchange mechanism, it then follows that the primary factor influencing exchange kinetics is the differing solubilities between pre- and postexchange materials.³⁹ Therefore, great insight on the exchange success can be obtained by an analysis of the structure of preand post-exchange materials.

SBC ([Ag(4,4'-bipy)][CrO₄]_{0.5}·3.5H₂O), which we denote SLUG-56 for University of California, Santa Cruz, Structure No. 56 (Figure 1a,b), crystallizes in the triclinic system with the $P\overline{1}$ space group. As with SBDC and SEC, the Ag atoms and organic linkers form 1D cationic polymer chains (Figure 1a,b). The polymers π – π stack into a column (Figure 1a,b), with an average centroid-to-centroid distance of 3.567(12) Å between

the pyridine rings (Table S2). ⁴⁰ Each chromate anion interacts with two Ag centers: one Ag–O interaction is shorter (2.555(2) Å) than the other (2.576(2) Å) (Table S2). The distance between Ag atoms ranges from 3.3629(5) to 3.3952(5) Å (Table S2), which are in the range of noncovalent long-contact interactions. Between the columns of π -stacked polymers reside the chromate anions, as well as 3.5 water molecules per Ag atom.

SBDC ([Ag(4,4'-bipy)][Cr₂O₇]_{0.5}·H₂O, SLUG-57) crystallizes in the monoclinic system with the I2/a space group (Figure 1c). The structure contains one Ag–Ag interaction, with a distance of 3.4197(7) Å. The structure displays $\pi - \pi$ stacking with an average distance of 3.606(2) Å between pyridine rings (Table S2). Furthermore, each dichromate anion interacts with two distinct Ag centers through a total of four Ag–O interactions ranging from 2.653(4) to 2.677(4) Å. Like SBC, the polymer chains stack into continuous columns with dichromate residing between said layers, as well as one water molecule per Ag atom. The structure is isostructural to SBP⁴¹ and SLUG-21⁴² [Ag₂(4,4'-bipy)₂(O₃SCH₂CH₂SO₃)] (the structures of which have been previously published) but with slightly shifted stacked polymer chains.

Like SBC, SEC ([Ag(4,4'-bpe)][CrO₄]_{0.5}, SLUG-58) crystallizes in the triclinic system with the $P\bar{1}$ space group (Figure 1d). The only Ag–Ag interaction is again at an extended distance of 3.3648(3) Å. Interestingly, the structure displays no π – π stacking; unlike SBC and SBDC, the polymer chains do not stack into continuous columns. Each chromate interacts with three Ag centers with Ag–O distances of 2.5678(18), 2.535(2), and 2.563(2) Å. There are no water molecules present within the structure, most likely due to the longer alkyl chain in the bpe ligand, leading to larger hydrophobic areas.

One notable factor potentially impacting the overall stability of said structures is the degree of $\pi-\pi$ stacking. SBC and SBDC both display a high level of $\pi-\pi$ stacking (Table S2), presumably leading to the enhanced stability of the structures. In contrast, SEC contains no $\pi-\pi$ stacking and the TGA data are consistent with SEC having less structural stability than SBC or SBDC (Figure S5). Additionally, SBDC has four Ag—O interactions per anion in comparison to two such interactions for SBC (Table S2). This may contribute to the increased structural stability of SBDC over SBC. The qualitative assessment of structural stability can be confirmed via $K_{\rm sp}$ (Table 1). SEC is the least stable (most soluble) of the three structures, followed by SBC and then SBDC as the most stable (least soluble) structure.

Table 1. Solubility and $K_{\rm sp}$ Values Obtained via ICP-OES for SBC, SBDC, and SEC

material	solubility (mmol/L)	$K_{\rm sp}~({ m M}^3)$
SBC	0.1578	3.93×10^{-12}
SBDC	0.0196	7.57×10^{-15}
SEC	0.1818	6.01×10^{-12}

3.2. Exchange Kinetics. The kinetics of Cr uptake by SBA, SBN, and SEN at pH 7 were investigated (Figure 2) and modeled with a pseudo-second-order kinetics model (Table 2). While the exchanges were also fit to a pseudo-first-order kinetics model, the R^2 values for SBA, SBN, and SEN (0.6496, 0.7061, and 0.9004, respectively) were notably lower than the respective R^2 values using the pseudo-second-order kinetics

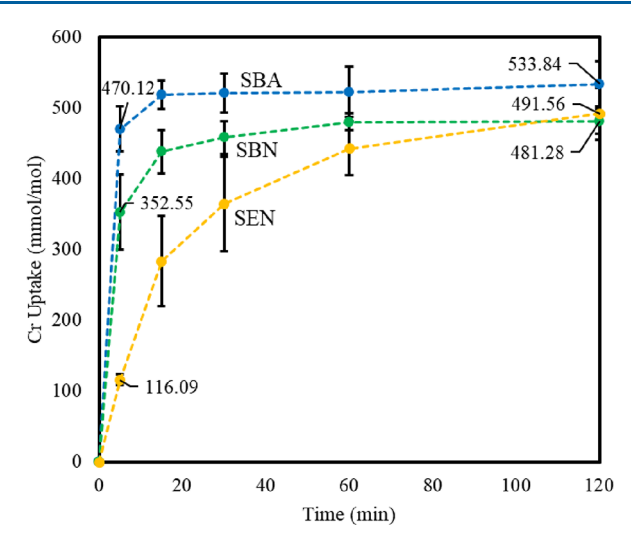


Figure 2. Cr uptake by SBA (blue), SBN (green), and SEN (gold) in millimoles per mole over 120 min. Exchange conditions were pH 7 and equimolar ratios of Cr to material (2.5 mM, 50 mL); aliquots were analyzed by UV—vis.

Table 2. Pseudo-Second-Order Kinetic Parameters

material	k_2 [g/mg·min]	$Q_{\rm e} \left[{\rm mg/g}\right]$	$h [mg/g \cdot min]$	R^2
SBA	0.0160	74.1	87.7	0.9999
SBN	0.0071	78.1	43.3	0.9999
SEN	0.0007	82.6	4.92	0.9987

model (Table 2). SBN was chosen for comparison to display the impacts of the starting anion in the exchange, while SEN was chosen as it is a Ag(I) CP with a similar organic linker to the SBX materials. While attempts were made to synthesize SEA, it did not readily form under the conditions as the other materials reported here.

SBA rapidly takes up Cr, reaching 470 mmol/mol in only 5 min, with an initial sorption rate of 87.7 mg/g·min (Table 2). The Cr uptake then quickly levels off in nearly 15 min before reaching equilibrium. Meanwhile, SBN requires close to 60 min to reach near equilibrium levels, with an initial sorption rate of only 43.3 mg/g·min (Table 2). It should be noted that while the uptake capacities, Q, of SBN and SEN are slightly higher than that of SBA, this apparent reversal is primarily due to the lighter formula weight of SBN and SEN in comparison to SBA (326.06, 354.12, and 377.16 g/mol, respectively). As shown in Figure 2, SBA has a significantly higher uptake of Cr in units of millimoles per mole and thus was chosen over SBN as the starting material for further exchange analysis. SEN requires over 120 min to approach equilibrium and has a much lower initial sorption rate of 4.92 mg/g·min (Table 2). Interestingly, by 120 min, SEN is observed to have greater Cr uptake than SBN, which will hopefully prompt further research of this material for anion exchange. The exchange for chromate was further confirmed via FT-IR (Figure S6).

As aqueous exchange is largely dictated by the differential solubilities in the starting and final material, the rapid and high-capacity exchange of SBA in comparison to SBN is likely due to the increased solubility of the acetate-containing material. We have previously reported that the $K_{\rm sp}$ of SBA is 1.25×10^{-7} M³ while that of SBN is 6.40×10^{-11} M³.³0 Both SBA and SBN, however, outperform the longer ligand material, SEN, in the initial sorption rate. This phenomenon is most likely due to the significantly higher level of $\pi-\pi$ stacking observed in SBC

in comparison to SEC (vide supra); the increased stability of SBC (the exchange product) will consequently increase the Cr exchange of SBA (Table 1).

3.3. Effect of pH on Exchange. Due to the wide range of acidity/alkalinity of industrial wastewaters, it is critical to test materials designed for the removal of aqueous pollutants at a variety of pH values. Indeed, the predominant species of Cr(VI) will vary depending on both concentration and pH (Figure 3). Thus, the uptake of Cr by SBA was studied

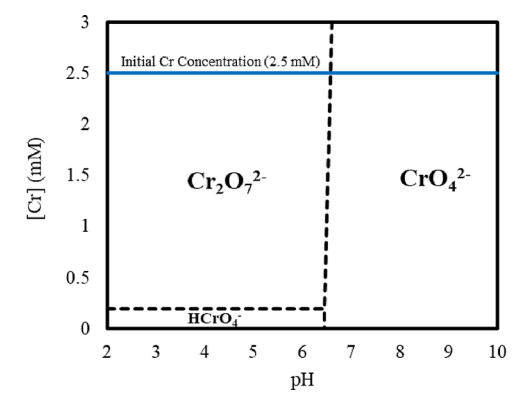


Figure 3. Cr speciation as a function of pH and concentration. Blue line represents the initial Cr(VI) concentration of 2.5 mM used for exchange experiments.

between pH 2 and pH 10. It should be noted that as the exchange studies were performed with an equimolar Cr(VI) and CP concentration of 2.5 mM, the predominant Cr species was dichromate $(Cr_2O_7^{2-})$ at acidic pH values and chromate (CrO_4^{2-}) at neutral or basic pH values.

SBA has an extremely high uptake of Cr at a range of pH values, reaching up to 968 mmol Cr(VI)/mol SBA (133 mg Cr/g) at pH 4 after 24 h with equimolar concentrations of SBA and Cr(VI) (Figure 4). The increased performance of Cr

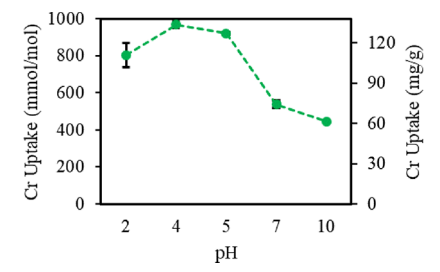


Figure 4. Cr(VI) uptake by SBA after 24 h at varying pH levels (via addition of sulfuric acid or sodium hydroxide), using equimolar exchange (2.5 mM) and determined via ICP-OES, in millimoles per mole and milligrams per gram.

exchange at more acidic pH values is both expected and desirable, as industrial wastewaters can be notably acidic. 14,43 Under these conditions, the predominant Cr species is dichromate, which theoretically allows for 1 mol of Cr (i.e., 0.5 mol of dichromate) uptake per mole of monovalent cationic material. At particularly acidic pH values (pH 2), the total Cr uptake of the material decreases slightly to 803 mmol/mol (111 mg Cr/g). This phenomenon likely arises from protonation of the 4,4′-bipy ligand, which has a p K_a value of 5, leading to CP breakdown. Similarly, as the pH becomes more alkaline, the Cr uptake also decreases, with an uptake of 536

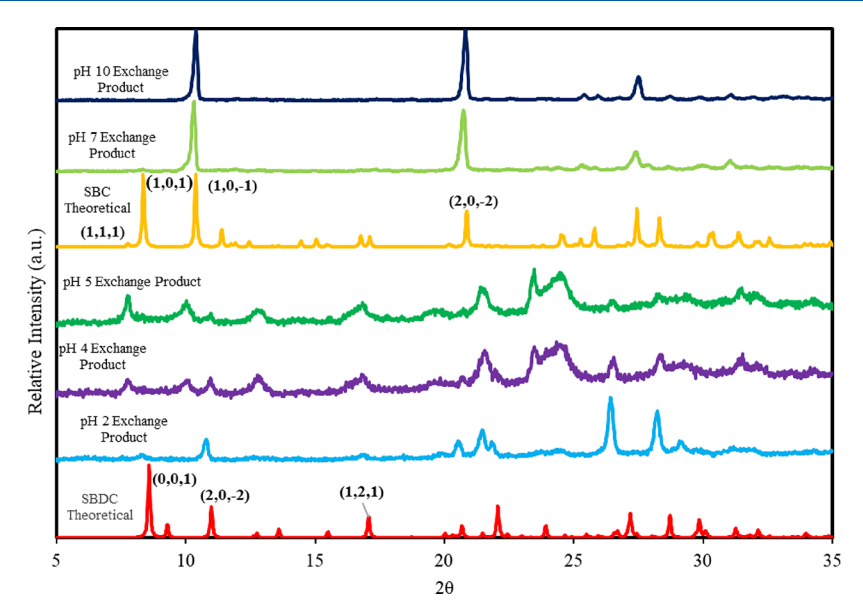


Figure 5. PXRD spectra of post-exchange products and theoretical patterns projected from the single crystal structures. For enhanced pH 7 and SBC theoretical spectra, see the Supporting Information (Figure S7).

mmol/mol (73.9 mg Cr/g) and 445 mmol/mol (61.4 mg Cr/g) at pH 7 and 10, respectively. We presume that this lower uptake arises from conversion of dichromate to chromate under basic conditions, limiting the potential uptake of Cr for monovalent anion-exchange materials (Figure 3).

All post-exchange materials were analyzed by PXRD (Figure 5). The powder diffractograms for the pH 7 and pH 10 postexchange product clearly match the theoretical PXRD predicted from the SCXRD data for SBC, with slight differences in intensity due to preferred orientation (Figure S7). The post-exchange materials from the pH 2, 4, and 5 exchange experiments roughly match the theoretical PXRD data for SBDC, with a notable drop in crystallinity. This reduction may be due to the presence of multiple phases within the bulk product that may stem from the potential uptake of hydrogen chromate (which will increase in predominance as the Cr concentration decreases over the course of the exchange, Figure 3) and the uptake of chromate, which becomes increasingly prevalent as the pH increases (Figure S8). The presence of multiple phases in the postexchange material is supported by the observation of two distinct dominant morphologies via SEM (Figure S3). To investigate the hypothesis that the second phase might arise from uptake of hydrogen chromate, we performed an exchange at pH 4 in the presence of a vast excess of Cr(VI), which would limit the concentration and, consequently, uptake of hydrogen chromate. The PXRD data of the post-exchange material obtained under these conditions matches the theoretical SBDC spectrum significantly better than the postexchange material of the equimolar pH 4 post-exchange material (Figure S8). The potential uptake of chromate can be observed as the pH increases. Particularly at pH 4 and 5, the resultant PXRD data show evidence for the presence of both SBC and SBDC (Figure S8). Decreased crystallinity may also be due to the possible presence of protonated 4,4'bipyridinium salts. These salts may be responsible for the two peaks at 26.5° and 28.4° (2 θ), which decrease in intensity as the acidity of the exchange medium decreases. Bipyridinium sulfate was synthesized and analyzed via PXRD but was determined to not be responsible for the unidentified peaks.

The product did not display any significantly large peaks beyond 30° (2θ), as would be characteristic of condensed silver chromate, silver dichromate, or silver oxides. ⁴⁴ Additionally, no uptake of Cr was observed after 24 h using the organic ligand only at pH 4, ensuring that the uptake of dichromate was not due to the formation of a protonated 4,4′-bipyridinium dichromate salt. Identification of all phases present within the bulk product beyond that of SBDC and SBC, however, will require further investigation.

3.4. Capacity. The capacity of SBA at pH 4 was determined by analyzing the uptake of Cr(VI), q_e , at varying initial Cr(VI) concentrations, C_v ranging from 25 to 517 ppm Cr(VI) (Figure 6). These data were then fit to a Langmuir

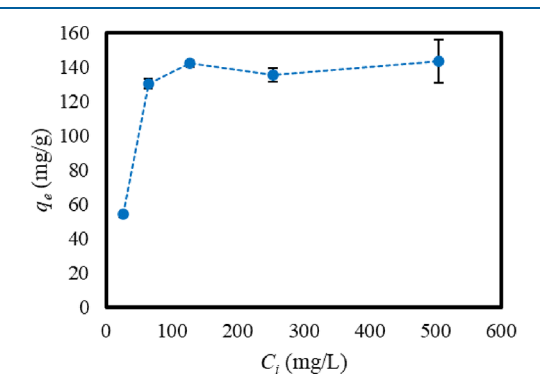


Figure 6. Cr(VI) uptake of SBA at pH 4, q_e , in milligrams per gram with varying initial Cr(VI) concentrations, C_{ij} in milligrams per liter.

model with an R^2 value of 0.9992 and to a Freundlich model with an R^2 value of 0.4727. Thus, the Langmuir model was chosen for further analysis. The Langmuir model reveals the maximum sorption capacity of SBA at pH 4 to be 143.0 mg Cr/g. This value is in good agreement with the theoretical maximum absorbance, 137.9 mg/g, which is calculated by assuming 1 mol of Cr per mole of SBA.

Despite the significant weight percentage of the silver metal (28.6% of total mass), SBA displays one of the highest Cr uptakes in milligrams per gram (143.0 mg/g) reported by CPs

to date. Comparators include, but are not limited to, $Zn_{0.5}Co_{0.5}$ -SLUG-35 (68.5 mg Cr/g), FIR-54 (49.6 mg Cr/g), and ABT·2ClO₄ (103 mg Cr/g). A full list of the Cr uptake capacities of published CPs is provided in Table S3. A full list of the Cr uptake are FJI-Cl1 (155 mg Cr/g). And UiO-66-based polymers (including but not limited to MOR-1, MOR-2, Form-UiO-66, and UiO-66-NH₂, which display Cr(VI) uptakes ranging between 117 and 244 mg/g, Table S3). FJI-Cl1 and UiO-66-based materials both require solvothermal synthesis methods (1:1 EtOH/water and DMF with HCl, respectively) and release chloride, limiting their potential application as remediators of environmental pollution. In contrast, SBA is prepared in water at room temperature and releases acetate, a non-toxic molecule.

Due to the cost of silver, the reversibility of exchange was explored, but the release of dichromate from SBDC cannot be meaningfully achieved even after 24 h in a pH 7 solution with 100-fold molar excess of sodium acetate. This is a testament to the remarkable stability of the SBDC complex. While further studies are needed to establish the conditions for SBA reuse, we note that the ability to strongly trap Cr(VI) is highly desired.

3.5. Kinetics. Given the extremely high uptake of dichromate by SBA at pH 4, the kinetics of the exchange were analyzed in an equimolar solution (Figure 7). Within as

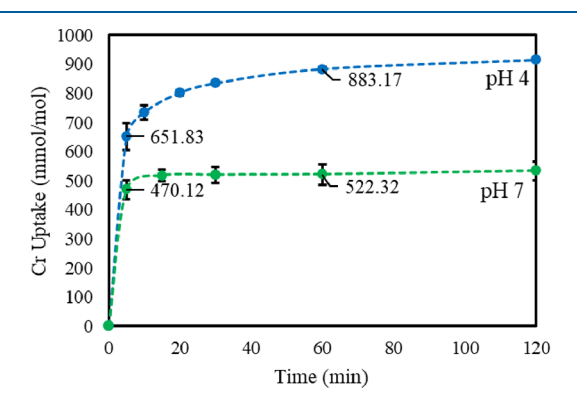


Figure 7. Cr uptake by SBA in millimoles per mole over 120 min. Exchange conditions were pH 4 and equimolar ratio of Cr to material (2.5 mM). pH 7 exchange curve also included for reference. Aliquots were analyzed via UV—vis.

little as 5 min, SBA reached a chromium uptake of 651 mmol/mol (90 Cr mg/g), and by 60 min, the chromium uptake was observed to be 883 mmol/mol (121 Cr mg/g). The exchange at pH 4 was again fit to a pseudo-second-order kinetic model with an R^2 value of 0.9998. The exchange has a calculated rate constant (k_2) of 0.00297 g/(mg·min), $Q_{\rm e}$ of 128.8 mg/g, and initial sorption rate of 49.2 mg/g·min. While SBA displays rapid Cr(VI) uptake at pH 4 during the initial 5 min of exchange, the kinetic parameters indicate that SBA requires longer to approach equilibrium at this pH value (Figure 7).

3.6. Selectivity. As mentioned previously, one of the challenges of removing Cr from wastewater is the presence of interfering anions, frequently nitrate and sulfate. Thus, in order to display the potential application of SBA as a mitigator of Cr pollution, the Cr exchange of SBA was tested in the presence of 50-fold excess molar aqueous concentrations of nitrate, sulfate, and carbonate (Figure 8). The material maintained its incredibly high uptake. With no competing

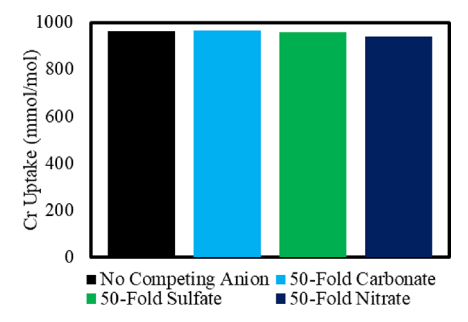


Figure 8. Cr uptake of SBA in millimoles per mole after 24 h in the presence of (from left to right) no competing anion, 50-fold molar excess carbonate, 50-fold molar excess sulfate, and 50-fold molar excess nitrate.

anion, SBA reaches an uptake of 963 mmol/mol (133 mg Cr/ g) under equimolar conditions, while the uptake remains at 100, 99.5, and 97.5% of the original in the presence of 50-fold molar excess of carbonate, sulfate, and nitrate, respectively. It should be noted that while uptake of Cr among a large molar excess of halides was tested, this led to the precipitation of insoluble silver halides. Selectivity within sulfate and nitrate is particularly pertinent, as these anions were the primary competing anions reported in Cr(VI)-polluted electroplating wastewater. 14 The high degree of selectivity of SBA makes it a particularly attractive material, even in comparison to other CPs. The Cr uptake of FJI-C11, for example, drops to 74% of its original value in only 12-fold excess of competing monovalent anions (F⁻, Cl⁻, Br⁻, and NO₃⁻).⁴⁷ While not all cited UiO-66-based materials report their selectivity, the Cr uptake of UiO-66-NH2@silica is lowered to 81 and 29% of its original value in the presence of 10-fold molar excess of nitrate and sulfate, respectively.⁵¹ Even MOR-2, which impressively maintains high Cr uptake in the presence of 1000-fold excess of monovalent anions (Cl⁻, Br⁻, and NO₃⁻), experiences a decrease in Cr(VI) uptake to 52% of its original value in the presence of a fourfold excess of sulfate.⁴⁸

Although it is difficult to compare CPs to covalent-organic frameworks (COFs) in terms of total Cr uptake in milligrams per gram due to the heavy weight fraction of the metal in CPs, COFs comparatively suffer in their selectivity, particularly in the presence of polyvalent anions. Tp-DG_{Cl}, for example, displays remarkable uptake of Cr (360 mg Cr/g), but the Cr uptake drops by approximately 60 and 80% in solutions containing sulfate in only 2-fold and 20-fold molar excess, respectively.

4. CONCLUSIONS

SBA was determined to display remarkably high Cr uptake among CP-type materials. Further, the material displays rapid kinetics and high selectivity, even in the presence of a great excess of competing anions. The material benefits from a onestep, scalable, green synthesis and additionally releases only acetate—an environmentally benign anion. Future study of SBA as a potential Cr pollution mitigator will require investigation into the scalability of the exchange as well as practical methods of implementation, such as column versus batch-based exchange, flow rate, and residence time.

ASSOCIATED CONTENT

Supporting Information

The Supporting Information is available free of charge at https://pubs.acs.org/doi/10.1021/acs.inorgchem.2c03110.

PXRD spectra of starting materials, UV—vis analysis of Cr uptake, SEM micrographs, structure views of SBA, SBN, and SEN, TGA analysis of materials, FT-IR of post-exchange products, PXRD spectra of pH 7 post-exchange product and SBC theoretical, PXRD analysis of SBDC products and SBDC theoretical, thermal ellipsoid plots of SLUG-56—58, crystallographic refinement details, tabulated structural parameters of SLUG-56—58, and list of published Cr uptakes for coordination polymer-type materials (PDF)

Accession Codes

CCDC 2204166–2204168 contain the supplementary crystallographic data for this paper. These data can be obtained free of charge via www.ccdc.cam.ac.uk/data_request/cif, or by emailing data_request/cif, or by contacting The Cambridge Crystallographic Data Centre, 12 Union Road, Cambridge CB2 1EZ, UK; fax: +44 1223 336033.

AUTHOR INFORMATION

Corresponding Author

Scott R. J. Oliver – Department of Chemistry and Biochemistry, University of California, Santa Cruz, Santa Cruz, California 95064, United States; oocid.org/0000-0002-6160-1518; Email: soliver@ucsc.edu

Authors

Cambell S. Conour — Department of Chemistry and Biochemistry, University of California, Santa Cruz, Santa Cruz, California 95064, United States; orcid.org/0000-0001-9170-6436

Daniel G. Droege — Department of Chemistry and Biochemistry, University of California, Santa Cruz, Santa Cruz, California 95064, United States; orcid.org/0000-0001-6165-6538

Beatriz Ehlke — Department of Chemistry and Biochemistry, University of California, Santa Cruz, Santa Cruz, California 95064, United States; ⊚ orcid.org/0000-0002-3973-1383

Timothy C. Johnstone – Department of Chemistry and Biochemistry, University of California, Santa Cruz, Santa Cruz, California 95064, United States; ◎ orcid.org/0000-0003-3615-4530

Complete contact information is available at: https://pubs.acs.org/10.1021/acs.inorgchem.2c03110

Author Contributions

The manuscript was written through contributions of all authors.

Funding

This work was partially supported by NSF PFI grant 2044692 and Supplement 2231436 for a summer REU in support of C.S.C.

Notes

The authors declare no competing financial interest.

ACKNOWLEDGMENTS

The single-crystal X-ray diffractometer housed in the UCSC X-ray Diffraction Facility was funded by NSF MRI grant

2018501. ICP-OES analysis was performed in the UC Santa Cruz Plasma Analytical Laboratory, RRID:SCR_021925, with assistance from Dr. Brian Dreyer. We acknowledge Dr. Tom Yuzvinsky for assistance with sample preparation and electron microscopy and the W.M. Keck Center for Nanoscale Optofluidics for use of the FEI Quanta 3D Dualbeam microscope. C.S.C. acknowledges the UCSC Undergraduate Research in Science & Technology Award in support of this research.

REFERENCES

- (1) Xia, S.; Song, Z.; Jeyakumar, P.; Shaheen, S. M.; Rinklebe, J.; Ok, Y. S.; Bolan, N.; Wang, H. A Critical Review on Bioremediation Technologies for Cr(VI)-Contaminated Soils and Wastewater. *Crit. Rev. Environ. Sci. Technol.* **2019**, *49*, 1027–1078.
- (2) Stern, C. M.; Jegede, T. O.; Hulse, V. A.; Elgrishi, N. Electrochemical Reduction of Cr(VI) in Water: Lessons Learned from Fundamental Studies and Applications. *Chem. Soc. Rev.* **2021**, *50*, 1642–1667.
- (3) Peng, H.; Guo, J. Removal of Chromium from Wastewater by Membrane Filtration, Chemical Precipitation, Ion Exchange, Adsorption Electrocoagulation, Electrochemical Reduction, Electrodialysis, Electrodeionization, Photocatalysis and Nanotechnology: A Review. *Environ. Chem. Lett.* **2020**, *18*, 2055–2068.
- (4) Tumolo, M.; Ancona, V.; De Paola, D.; Losacco, D.; Campanale, C.; Massarelli, C.; Uricchio, V. F. Chromium Pollution in European Water, Sources, Health Risk, and Remediation Strategies: An Overview. *Int. J. Environ. Res. Public Health* **2020**, *17*, 5438.
- (5) Zhuang, X.; Hao, J.; Zheng, X.; Fu, D.; Mo, P.; Jin, Y.; Chen, P.; Liu, H.; Liu, G.; Lv, W. High-Performance Adsorption of Chromate by Hydrazone-Linked Guanidinium-Based Ionic Covalent Organic Frameworks: Selective Ion Exchange. Sep. Purif. Technol. 2021, 274, No. 118993.
- (6) Fei, H.; Han, C. S.; Robins, J. C.; Oliver, S. R. J. A Cationic Metal—Organic Solid Solution Based on Co(II) and Zn(II) for Chromate Trapping. *Chem. Mater.* **2013**, *25*, 647–652.
- (7) Barakat, M. A. New Trends in Removing Heavy Metals from Industrial Wastewater. *Arab. J. Chem.* **2011**, *4*, 361–377.
- (8) Mohan, D.; Pittman, C. U. Activated Carbons and Low Cost Adsorbents for Remediation of Tri- and Hexavalent Chromium from Water. J. Hazard. Mater. 2006, 137, 762–811.
- (9) Zhitkovich, A. Chromium in Drinking Water: Sources, Metabolism, and Cancer Risks. *Chem. Res. Toxicol.* **2011**, 24, 1617–1629
- (10) Zhang, B.; Luan, L.; Gao, R.; Li, F.; Li, Y.; Wu, T. Rapid and Effective Removal of Cr(VI) from Aqueous Solution Using Exfoliated LDH Nanosheets. *Colloids Surf., A* **2017**, *520*, 399–408.
- (11) Pavesi, T.; Moreira, J. C. Mechanisms and Individuality in Chromium Toxicity in Humans. *J. Appl. Toxicol.* **2020**, *40*, 1183–1197
- (12) Miretzky, P.; Cirelli, A. F. Cr(VI) and Cr(III) Removal from Aqueous Solution by Raw and Modified Lignocellulosic Materials: A Review. *J. Hazard. Mater.* **2010**, *180*, 1–19.
- (13) Izak, P.; Hrma, P.; Arey, B. W.; Plaisted, T. J. Effect of Feed Melting, Temperature History, and Minor Component Addition on Spinel Crystallization in High-Level Waste Glass. *J. Non-Cryst. Solids* **2001**, 289, 17–29.
- (14) Cao, W.; Dang, Z.; Yi, X.-Y.; Yang, C.; Lu, G.-N.; Liu, Y.-F.; Huang, S.-Y.; Zheng, L.-C. Removal of Chromium (VI) from Electroplating Wastewater Using an Anion Exchanger Derived from Rice Straw. *Environ. Technol.* **2013**, *34*, 7–14.
- (15) Custelcean, R. Anions in Crystal Engineering. *Chem. Soc. Rev.* **2010**, 39, 3675–3685.
- (16) Ahamed, M. I. N.; Rajeshkumar, S.; Ragul, V.; Anand, S.; Kaviyarasu, K. Chromium Remediation and Toxicity Assessment of Nano Zerovalent Iron against Contaminated Lake Water Sample (Puliyanthangal Lake, Tamilnadu, India). S. Afr. J. Chem. Eng. 2018, 25, 128–132.

- (17) Custelcean, R. Urea-Functionalized Crystalline Capsules for Recognition and Separation of Tetrahedral Oxoanions. *Chem. Commun.* **2013**, 49, 2173–2182.
- (18) Citrak, S. C.; Popple, D.; Delgado-Cunningham, K.; Tabler, K.; Bdeir, K.; Oliver, A. G.; Kvam, P. B.; Oliver, S. R. J. Extremely Rapid Uptake of Perchlorate with Release of an Environmentally Benign Anion: Silver Bipyridine Acetate. *Cryst. Growth Des.* **2018**, *18*, 1891–1895.
- (19) Custelcean, R.; Moyer, B. A. Anion Separation with Metal-Organic Frameworks. Eur. J. Inorg. Chem. 2007, 2007, 1321–1340.
- (20) Cheetham, A. K.; Rao, C. N. R.; Feller, R. K. Structural Diversity and Chemical Trends in Hybrid Inorganic—Organic Framework Materials. *Chem. Commun.* **2006**, 4780–4795.
- (21) Tran, D. T.; Zavalij, P. Y.; Oliver, S. R. J. Pb₃F₅NO₃, a Cationic Layered Material for Anion-Exchange. *J. Am. Chem. Soc.* **2002**, *124*, 3966–3969.
- (22) Colinas, I. R.; Silva, R. C.; Oliver, S. R. J. Reversible, Selective Trapping of Perchlorate from Water in Record Capacity by a Cationic Metal—Organic Framework. *Environ. Sci. Technol.* **2016**, *50*, 1949—1954.
- (23) Kitagawa, S.; Kitaura, R.; Noro, S. Functional Porous Coordination Polymers. *Angew. Chem., Int. Ed.* **2004**, *43*, 2334–2375. (24) He, L.; Liu, S.; Chen, L.; Dai, X.; Li, J.; Zhang, M.; Ma, F.; Zhang, C.; Yang, Z.; Zhou, R.; Chai, Z.; Wang, S. Mechanism Unravelling for Ultrafast and Selective ⁹⁹TcO₄⁻ Uptake by a Radiation-Resistant Cationic Covalent Organic Framework: A Combined Radiological Experiment and Molecular Dynamics Simulation Study. *Chem. Sci.* **2019**, *10*, 4293–4305.
- (25) Li, Y.; Yang, Z.; Wang, Y.; Bai, Z.; Zheng, T.; Dai, X.; Liu, S.; Gui, D.; Liu, W.; Chen, M.; Chen, L.; Diwu, J.; Zhu, L.; Zhou, R.; Chai, Z.; Albrecht-Schmitt, T. E.; Wang, S. A Mesoporous Cationic Thorium-Organic Framework That Rapidly Traps Anionic Persistent Organic Pollutants. *Nat. Commun.* **2017**, *8*, 1354.
- (26) Drout, R. J.; Otake, K.; Howarth, A. J.; Islamoglu, T.; Zhu, L.; Xiao, C.; Wang, S.; Farha, O. K. Efficient Capture of Perrhenate and Pertechnetate by a Mesoporous Zr Metal—Organic Framework and Examination of Anion Binding Motifs. *Chem. Mater.* **2018**, *30*, 1277—1284.
- (27) Li, J.; Dai, X.; Zhu, L.; Xu, C.; Zhang, D.; Silver, M. A.; Li, P.; Chen, L.; Li, Y.; Zuo, D.; Zhang, H.; Xiao, C.; Chen, J.; Diwu, J.; Farha, O. K.; Albrecht-Schmitt, T. E.; Chai, Z.; Wang, S. ⁹⁹TcO₄⁻ Remediation by a Cationic Polymeric Network. *Nat. Commun.* **2018**, *9*, 3007.
- (28) Rapti, S.; Diamantis, S. A.; Dafnomili, A.; Pournara, A.; Skliri, E.; Armatas, G. S.; Tsipis, A. C.; Spanopoulos, I.; Malliakas, C. D.; Kanatzidis, M. G.; Plakatouras, J. C.; Noli, F.; Lazarides, T.; Manos, M. J. Exceptional TcO⁴⁻ Sorption Capacity and Highly Efficient ReO⁴⁻ Luminescence Sensing by Zr⁴⁺ MOFs. *J. Mater. Chem. A* **2018**, *6*, 20813–20821.
- (29) Sheng, D.; Zhu, L.; Xu, C.; Xiao, C.; Wang, Y.; Wang, Y.; Chen, L.; Diwu, J.; Chen, J.; Chai, Z.; Albrecht-Schmitt, T. E.; Wang, S. Efficient and Selective Uptake of TcO⁴⁻ by a Cationic Metal—Organic Framework Material with Open Ag⁺ Sites. *Environ. Sci. Technol.* **2017**, *51*, 3471–3479.
- (30) Citrak, S. C.; Bdeir, K.; Delgado-Cunningham, K.; Popple, D.; Oliver, S. R. J. Exchange Capability of Cationic Silver 4,4'-Bipyrdine Materials for Potential Water Remediation: Structure, Stability, and Anion Exchange Properties. *Inorg. Chem.* **2019**, *58*, 7189–7199.
- (31) Zhu, L.; Xiao, C.; Dai, X.; Li, J.; Gui, D.; Sheng, D.; Chen, L.; Zhou, R.; Chai, Z.; Albrecht-Schmitt, T. E.; Wang, S. Exceptional Perrhenate/Pertechnetate Uptake and Subsequent Immobilization by a Low-Dimensional Cationic Coordination Polymer: Overcoming the Hofmeister Bias Selectivity. *Environ. Sci. Technol. Lett.* **2017**, *4*, 316–322.
- (32) Yaghi, O. M.; Li, H. T-Shaped Molecular Building Units in the Porous Structure of Ag(4,4'-Bpy)·NO₃. *J. Am. Chem. Soc.* **1996**, *118*, 295–296.
- (33) LaDuca, R. L.; Rarig, R. S.; Zapf, P. J.; Zubieta, J. Ag (I)—Organodiimine Coordination Complex Polymers: Structural Influen-

- ces of Ligand Geometries and Charge-Compensating Oxoanions. Solid State Sci. 2000, 2, 39–45.
- (34) Rigaku Oxford Diffraction CrysAlisPro software system, version 1.171.40.78a; Rigaku Corporation: Wroclaw, Poland, 2020.
- (35) Sheldrick, G. M. SHELXT Integrated Space-Group and Crystal-Structure Determination. Acta Crystallogr., Sect. A: Found. Adv. **2015**, 71, 3–8.
- (36) Sheldrick, G. M. Crystal Structure Refinement with SHELXL. Acta Crystallogr., Sect. C: Struct. Chem. 2015, 71, 3–8.
- (37) Dolomanov, O. V.; Bourhis, L. J.; Gildea, R. J.; Howard, J. A.; Puschmann, H. *OLEX2*: A Complete Structure Solution, Refinement and Analysis Program. *J. Appl. Crystallogr.* **2009**, *42*, 339–341.
- (38) Müller, P. Practical Suggestions for Better Crystal Structures. *Crystallogr. Rev.* **2009**, *15*, 57–83.
- (39) Khlobystov, A. N.; Champness, N. R.; Roberts, C. J.; Tendler, S. J. B.; Thompson, C.; Schröder, M. Anion Exchange in Co-Ordination Polymers: A Solid-State or a Solvent-Mediated Process? *CrystEngComm* **2002**, *4*, 426–431.
- (40) Janiak, C. A Critical Account on $\pi-\pi$ Stacking in Metal Complexes with Aromatic Nitrogen-Containing Ligands. *J. Chem. Soc., Dalton Trans.* **2000**, 21, 3885–3896.
- (41) Wang, L.-S.; Zhang, J.-F.; Yang, S.-P. Catena-Poly-[[Silver(I)- μ -4,4'-Bi-pyridine- $_{\rm K}$ ²N:N'] Perchlorate]. *Acta Crystallogr., Sect. E: Struct. Rep. Online* **2004**, *60*, m1484—m1486.
- (42) Fei, H.; Paw, U.; Rogow, D. L.; Bresler, M. R.; Abdollahian, Y. A.; Oliver, S. R. J. Synthesis, Characterization, and Catalytic Application of a Cationic Metal–Organic Framework: Ag₂(4,4′-Bipy)₂(O₃SCH₂CH₂SO₃). *Chem. Mater.* **2010**, 22, 2027–2032.
- (43) Akbal, F.; Camci, S. Copper, Chromium and Nickel Removal from Metal Plating Wastewater by Electrocoagulation. *Desalination* **2011**, 269, 214–222.
- (44) Fowsiya, J.; Madhumitha, G. Biomolecules Derived from Carissa edulis for the Microwave Assisted Synthesis of Ag₂O Nanoparticles: A Study Against S. incertulas, C. medinalis and S. mauritia. J. Cluster Sci. 2019, 30, 1243–1252.
- (45) Fu, H.-R.; Xu, Z.-X.; Zhang, J. Water-Stable Metal—Organic Frameworks for Fast and High Dichromate Trapping via Single-Crystal-to-Single-Crystal Ion Exchange. *Chem. Mater.* **2015**, 27, 205—210.
- (46) Li, X.; Xu, H.; Kong, F.; Wang, R. A Cationic Metal—Organic Framework Consisting of Nanoscale Cages: Capture, Separation, and Luminescent Probing of ${\rm Cr_2O_7}^{2-}$ through a Single-Crystal to Single-Crystal Process. *Angew. Chem., Int. Ed.* **2013**, *52*, 13769–13773.
- (47) Zou, Y.-H.; Liang, J.; He, C.; Huang, Y.-B.; Cao, R. A Mesoporous Cationic Metal—Organic Framework with a High Density of Positive Charge for Enhanced Removal of Dichromate from Water. *Dalton Trans.* **2019**, *48*, 6680–6684.
- (48) Rapti, S.; Sarma, D.; Diamantis, A.; Skliri, E.; Armatas, S.; Tsipis, C.; Hassan, S.; Alkordi, M.; Malliakas, D.; Kanatzidis, G.; Lazarides, T.; Plakatouras, C.; Manos, J. All in One Porous Material: Exceptional Sorption and Selective Sensing of Hexavalent Chromium by Using a Zr⁴⁺ MOF. *J. Mater. Chem. A* **2017**, *5*, 14707–14719.
- (49) Wang, Y.; Zhang, N.; Chen, D.; Ma, D.; Liu, G.; Zou, X.; Chen, Y.; Shu, R.; Song, Q.; Lv, W. Facile Synthesis of Acid-Modified UiO-66 to Enhance the Removal of Cr(VI) from Aqueous Solutions. *Sci. Total Environ.* **2019**, *682*, 118–127.
- (50) Ibrahim, A. H.; El-Mehalmey, W. A.; Haikal, R. R.; Safy, M. E. A.; Amin, M.; Shatla, H. R.; Karakalos, S. G.; Alkordi, M. H. Tuning the Chemical Environment within the UiO-66-NH₂ Nanocages for Charge-Dependent Contaminant Uptake and Selectivity. *Inorg. Chem.* **2019**, *58*, 15078–15087.
- (51) El-Mehalmey, W. A.; Ibrahim, A. H.; Abugable, A. A.; Hassan, M. H.; Haikal, R. R.; Karakalos, S. G.; Zaki, O.; Alkordi, M. H. Metal—Organic Framework@silica as a Stationary Phase Sorbent for Rapid and Cost-Effective Removal of Hexavalent Chromium. *J. Mater. Chem. A* 2018, *6*, 2742—2751.
- (52) Zhang, Q.; Yu, J.; Cai, J.; Zhang, L.; Cui, Y.; Yang, Y.; Chen, B.; Qian, G. A Porous Zr-Cluster-Based Cationic Metal-Organic

Framework for Highly Efficient $Cr_2O_7^{2-}$ Removal from Water. *Chem. Commun.* **2015**, *51*, 14732–14734.

- (53) Deng, S.-Q.; Mo, X.-J.; Zheng, S.-R.; Jin, X.; Gao, Y.; Cai, S.-L.; Fan, J.; Zhang, W.-G. Hydrolytically Stable Nanotubular Cationic Metal—Organic Framework for Rapid and Efficient Removal of Toxic Oxo-Anions and Dyes from Water. *Inorg. Chem.* **2019**, *58*, 2899—2909.
- (54) Zhang, C.; Liu, Y.; Sun, L.; Shi, H.; Shi, C.; Liang, Z.; Li, J. A Zwitterionic Ligand-Based Cationic Metal-Organic Framework for Rapidly Selective Dye Capture and Highly Efficient Cr₂O₇²⁻ Removal. *Chem. Eur. J.* **2018**, *24*, 2718–2724.
- (55) Ding, B.; Guo, C.; Xin Liu, S.; Cheng, Y.; Xia, W.; Mei Su, X.; Yuan Liu, Y.; Li, Y. A Unique Multi-Functional Cationic Luminescent Metal—Organic Nanotube for Highly Sensitive Detection of Dichromate and Selective High Capacity Adsorption of Congo Red. *RSC Adv.* **2016**, *6*, 33888–33900.
- (56) Desai, A. V.; Manna, B.; Karmakar, A.; Sahu, A.; Ghosh, S. K. A Water-Stable Cationic Metal—Organic Framework as a Dual Adsorbent of Oxoanion Pollutants. *Angew. Chem., Int. Ed.* **2016**, *55*, 7811—7815.
- (57) Zheng, T.-R.; Qian, L.-L.; Li, M.; Wang, Z.-X.; Li, K.; Zhang, Y.-Q.; Li, B.-L.; Wu, B. A Bifunctional Cationic Metal—Organic Framework Based on Unprecedented Nonanuclear Copper(II) Cluster for High Dichromate and Chromate Trapping and Highly Efficient Photocatalytic Degradation of Organic Dyes under Visible Light Irradiation. *Dalton Trans.* 2018, 47, 9103—9113.
- (58) Lv, X.-X.; Shi, L.-L.; Li, K.; Li, B.-L.; Li, H.-Y. An Unusual Porous Cationic Metal—Organic Framework Based on a Tetranuclear Hydroxyl-Copper(II) Cluster for Fast and Highly Efficient Dichromate Trapping through a Single-Crystal to Single-Crystal Process. Chem. Commun. 2017, 53, 1860–1863.
- (59) Ma, L.; Yang, J.; Lu, B.-B.; Li, C.-P.; Ma, J.-F. Water-Stable Metal-Organic Framework for Effective and Selective ${\rm Cr_2O_7}^{2-}$ Capture through Single-Crystal to Single-Crystal Anion Exchange. *Inorg. Chem.* **2018**, *57*, 11746–11752.
- (60) Li, L.-L.; Feng, X.-Q.; Han, R.-P.; Zang, S.-Q.; Yang, G. Cr(VI) Removal via Anion Exchange on a Silver-Triazolate MOF. *J. Hazard. Mater.* **2017**, 321, 622–628.
- (61) Shi, P.-F.; Zhao, B.; Xiong, G.; Hou, Y.-L.; Cheng, P. Fast Capture and Separation of, and Luminescent Probe for, Pollutant Chromate Using a Multi-Functional Cationic Heterometal-Organic Framework. *Chem. Commun.* **2012**, *48*, 8231–8233.

☐ Recommended by ACS

Replenishment in the Family of Rhenium Chalcobromides; Synthesis and Structure of Molecular $\{Re_4S_4\}Br_8(TeBr_2)_4$, Dimeric $\{Re_4S_4\}Br_8(TeBr_2)_3\}_2$, and Polymeric $\{Re_4S_4\}B...$

Spartak S. Yarovoy, Nikolay G. Naumov, et al.

DECEMBER 05, 2022 INORGANIC CHEMISTRY

READ 🗹

$Gold(I)\cdots Lanthanide(III)$ Bonds in Discrete Heterobimetallic Compounds: A Combined Computational and Topological Study

Daniel Blasco and Dage Sundholm

DECEMBER 07, 2022

INORGANIC CHEMISTRY

READ **C**

 $Two \ [Co(bipy)_3]^{3+} - Templated \ Silver \ Halobismuthate \\ Hybrids: \ Syntheses, \ Structures, \ Photocurrent \ Responses, \ and \\ Theoretical \ Studies$

Bo Zhang, Meng-Zhen Liu, et al.

JUNE 10, 2022 INORGANIC CHEMISTRY

READ 🗹

Functionalizing Carbon Nanotubes with Bis(2,9-dialkyl-1,10-phenanthroline)copper(II) Complexes for the Oxygen Reduction Reaction

Deborah Brazzolotto, Alan Le Goff, et al.

SEPTEMBER 15, 2022

INORGANIC CHEMISTRY

READ 🗹